



# Identification, isolation, and characterization of a novel type of Fukushima-derived microparticle

Zsuzsanna Macsik<sup>1</sup> · Lisa A. Hudston<sup>1</sup> · Kimberly N. Wurth<sup>1</sup> · Daniel Meininger<sup>1</sup> · Christian Jesinghaus<sup>1,2</sup> · Travis J. Tenner<sup>1</sup> · Benjamin E. Naes<sup>1</sup> · Mitzi Boswell<sup>1</sup> · Katsumi Shozugawa<sup>3</sup> · Stephen P. LaMont<sup>1</sup> · Robert E. Steiner<sup>1</sup> · Georg Steinhauser<sup>4,1,5</sup>

Received: 10 May 2022 / Accepted: 11 September 2022 / Published online: 11 November 2022  
© The Author(s) 2022

## Abstract

In the course of the Fukushima nuclear accident, radionuclides were released in various forms, including so-called radio-cesium-bearing microparticles (CsMP). So far, four types of CsMP were described: Type A is smaller in size (<10 μm), Types B, C, and D are larger (>100 μm). In this work, we present a novel type of CsMP (proclaimed Type E). Three particles of Type E were extracted from a contaminated blade of grass that was sampled 1.5 km from the Fukushima Daiichi nuclear power plant in late 2011. They were located using autoradiography, isolated using an optical microscope and micromanipulator, and characterized using scanning electron microscopy, energy dispersive x-ray spectroscopy, and low-level gamma-ray spectrometry. Type E CsMPs are 10–20 μm in size and exhibit an unusually low and barely detectable <sup>137</sup>Cs activity of only ≤ 10 mBq per particle. Their brittle and fragile character may indicate a high surface tension.

**Keywords** Fukushima · Microparticles · Cesium-rich granule · <sup>137</sup>Cs · Environmental radioactivity

## Introduction

In the course of the Fukushima nuclear accident (Japan, March 11, 2011), large amounts of (mostly volatile) radionuclides were released into the environment [1]. These emissions included foremost all nuclides of iodine (I), tellurium (Te), and cesium (Cs). Of all the radionuclides, only

the two radiocesium isotopes <sup>134</sup>Cs ( $T_{1/2} = 2.01$  y) and especially <sup>137</sup>Cs ( $T_{1/2} = 30.08$  y) are relevant for long-term radio-protection considerations. Quite recently, long-lived <sup>135</sup>Cs ( $T_{1/2} = 2.3 \cdot 10^6$  y) has attracted interest for environmental sciences, as it allows for the identification of a source via its distinct <sup>135</sup>Cs/<sup>137</sup>Cs ratio [2–5]. Unfortunately, analysis of this ratio by desktop mass spectrometry requires relatively high activities/amounts of both radionuclides and is challenging for ultratrace levels. Release estimates for <sup>137</sup>Cs range from 6.1 to 15 PBq [6], 13 PBq [7], 17 PBq [8] to 20.1–53.1 PBq [9]. Initially, the average <sup>134</sup>Cs/<sup>137</sup>Cs ratio was about 0.98 [10]. Today, <sup>134</sup>Cs is only detectable in highly contaminated samples. Especially in contrast to the Chernobyl nuclear accident, which led to the emission of highly radioactive fuel particles, it is fair to say that today Fukushima has become mostly “a <sup>137</sup>Cs problem.”

However, the releases from the Fukushima Daiichi nuclear power plant (FDNPP) also included radioactive particles that have been termed Cs-bearing microparticles (CsMP) or granules that are distinct from those emitted from Chernobyl [11–14]. They were first described in Japanese literature [15, 16] followed by a report from Adachi et al. in international literature [17]. The matrix of these particles consists mostly of light elements (Si, O, C), but

Notice this is a part of a special issue!! SI: Methods and Applications of Radioanalytical Chemistry (MARC XII)

✉ Georg Steinhauser  
steinhauser@irs.uni-hannover.de;  
georg.steinhauser@tuwien.ac.at

<sup>1</sup> Nuclear and Radiochemistry Group, Chemistry Division, Los Alamos National Laboratory, 87545 Los Alamos, NM, USA

<sup>2</sup> Faculty of Electrical Engineering and Computer Science, Leibniz Universität Hannover, 30167 Hannover, Germany

<sup>3</sup> Graduate School of Art and Sciences, The University of Tokyo, Meguro-Ku, Tokyo, Japan

<sup>4</sup> Institute of Radioecology and Radiation Protection, Leibniz Universität Hannover, 30419 Hannover, Germany

<sup>5</sup> Institute of Applied Synthetic Chemistry & TRIGA Center Atominsttit, TU Wien, 1060 Vienna, Austria

heavier components such as Cs [18] and inclusions of actinides have also been described [19–21]. They are characterized by low solubility in water as well as a variety of reagents [22]. Although CsMP contain significant amounts of radiocesium, the radiocesium trapped in these particles behaves much differently from depositions of volatile Cs species, which is much more bioavailable. Their low solubility makes CsMPs a long-lasting radiological hazard for environmental and human health for many years to come, especially in case of incorporation of a particle. Beyond any radiological hazards, CsMP are worthy object of study as they likely originate from the reactors' interior and hence offer potentially useful forensic information on the accident itself. Some of this information may ultimately contribute to a better understanding of the Fukushima nuclear accident. The origin of the particles is not completely understood, but there are credible reports showing that the particles' matrix is consistent with the composition of rockwool that was used as insulation material inside FDNPP [23]. Another report indicated that the particles were formed by the melting of glass fibers of the high-efficiency particulate air filter in the Standby Gas Treatment System in the course of the hydrogen explosions in FDNPP [24]. It is assumed that the particles were formed in the early stages of the accident [25]. Experiments showed that heating glass fibers to 450–800 °C formed microparticles similar in shape and composition to Fukushima-derived particles [26].

There have been attempts to categorize the particles by size, shape, activity, and elemental/isotopic composition [27]. Type A CsMPs have a mostly spherical shape, a size of < 10 µm, and  $^{137}\text{Cs}$  activities of 0.1–20 Bq per particle [18, 27, 28]. Based on the  $^{134}\text{Cs}/^{137}\text{Cs}$  activity ratio of ~1 (decay-corrected to the time of the accident), it was concluded that Type A particles originated from FDNPP Unit 2 [24] or Units 2 or 3 [18, 29]. Their Cs content is sufficiently high that it can be detected by scanning electron microscopy – energy dispersive x-ray spectroscopy (SEM-EDS).

Microparticles of Type B are much larger than Type A CsMPs (mostly 100–400 µm, sometimes 40–100 µm) [27], they have a non-uniform shape and contain activities  $^{137}\text{Cs}$  in the range of 30 to 100 Bq per particle [30], thus exhibiting a lower specific activity than Type A. Their  $^{134}\text{Cs}/^{137}\text{Cs}$  activity ratio is ~0.9 (as of March 11, 2011), pointing at FDNPP Unit 1 as the most likely source [31]. Apart from radiocesium, they also contain detectable activities of  $^{125}\text{Sb}$  [27]. The total Cs (stable and radioactive Cs) concentration is lower than in Type A CsMP and, hence, using nano- or microanalytical techniques, it can only be determined by synchrotron x-ray fluorescence spectroscopy.

Type C microparticles may or may not constitute a separate category of Fukushima-derived microparticles. At present, only one specimen has been described [32]. It has been

found in close vicinity to FDNPP. This Type C microparticle resembled Type B microparticles in terms of shape (non-spherical), size (120 µm), and (specific)  $^{137}\text{Cs}$  activity (224 Bq), but differed with its  $^{134}\text{Cs}/^{137}\text{Cs}$  ratio of ~1 (which was rather expected for Type A microparticles).

More recently, a novel type of particle was discovered in the vicinity of FDNPP [33]: Large (> 500 µm), glassy carbon particles with other micro-particles embedded into the surface. Their radiocesium activity exceeds  $10^6$  Bq  $^{134+137}\text{Cs}$  per particle. Their  $^{134}\text{Cs}/^{137}\text{Cs}$  ratio was reported 0.971 and 0.954, respectively [33], which correlates with the isotopic signature of Unit 1. Although they have not been named as such by the authors, they could be classified as Type D.

Various interesting observations were made lately, for example nanoparticulate Pu inclusions in CsMP [34]. Various methods have been tested to localize radioactive particles, especially uranium-bearing particles, including  $\alpha$ -tracks [35], fission tracks, imaging plates, and real time autoradiography [36, 37] or scanning electron microscopy (SEM) in backscattered electrons mode [38]. In this study, we investigated grass from Fukushima prefecture by autoradiography for possible presence of microparticles.

## Materials and methods

### Samples

Grass/vegetation samples were randomly collected on December 21, 2011, in Fukushima prefecture, Japan, about 1.5 km west-southwest from the FDNPP (37.417635 N, 141.012247 E). It is the same sample batch that was used in previous  $^{90}\text{Sr}$  [39] and Pu studies [40]. The sample code in those previous studies was B-V. The bulk activity concentrations (reference date: March 11, 2011) in this grass sample were  $142 \text{ Bq}\cdot\text{g}^{-1}$   $^{137}\text{Cs}$ ,  $130 \text{ Bq}\cdot\text{g}^{-1}$   $^{134}\text{Cs}$ , and  $0.39 \text{ Bq}\cdot\text{g}^{-1}$   $^{90}\text{Sr}$  [39]. The sample did not contain any detectable traces of Pu [40]. The sample was air-dried in 2011, but remained otherwise unaltered and was put on storage over the past decade.

### Autoradiography

For the present study, blades of grass were randomly selected from the bulk for autoradiographic imaging. Autoradiography is a non-destructive qualitative analysis technique that provides information about the location and relative intensity of radioactivity for a sample. The analysis system is comprised of phosphor imaging films and a low energy laser scanning system. Los Alamos National Laboratory (LANL) uses Fujifilm BAS-SR imaging films and an Amersham<sup>®</sup> Typhoon<sup>®</sup> scanner. An exposure of 30 h yielded the most suitable image.

## Particle extraction

Three particles from hot spot J were identified using an Olympus SZX16 optical microscope equipped with a camera. The microscope is located inside a radiological fume hood and equipped with a right-handed Micro Support Quick Pro micromanipulator. This allows for safe operation from outside the fume hood with a touch screen or mouse. Particle isolation was operated in real-time from the computer monitor. Each particle was picked with a 1  $\mu\text{m}$  tungsten needle and transferred to a clean silicon wafer. To increase the stickiness of the particle to the needle, the tip was rolled on Scotch™ permanent double-sided tape prior to particle picking. After picking, the particles were each transferred onto a clean silicon wafer for further SEM-EDS investigation as well as for gamma-ray spectroscopy.

## SEM-EDS

The three particles were analyzed using an FEI Quanta 200 F field emission SEM coupled with an energy dispersive X-ray analysis (EDAX; AMETEK brand) Octane silicon drift energy dispersive spectroscopy (EDS) detector. EDS data were collected and processed using EDAX TEAM software. All samples were imaged and measured at a variety of accelerating voltages (5 kV – 20 kV) and a spot size of 5 (large spot size optimal for EDS). Lower accelerating voltages were chosen to assist in isolating the particle signal from the substrate but limited the ability to detect higher atomic number elements. Larger accelerating voltages allowed detection of a wider range of elements in the sample but increased the interaction volume of the electron beam so that signal from the substrate was included in the analyses. This issue made it difficult to attain complete and accurate spectra from the samples.

Two EDS element maps were generated for sample 2. The first EDS map was taken at 5 kV with a smaller spot size of 3, EDS settings were as follows: amp time of 0.12  $\mu\text{s}$ , dwell time of 100  $\mu\text{s}$ , 128 frames (number of passes), total analysis time of  $\sim 5$  h. For this map, the 5 kV accelerating voltage and smaller spot size settings were chosen to resolve inclusions on the surface of the particle. The smaller spot size also assisted in mitigating sample drift. The 0.12  $\mu\text{s}$  amp time setting is the recommended value for EDS mapping in the TEAM software, however this setting resulted in lower atomic number elements (such as carbon) being excluded from the resulting spectrum and map. The second map was taken at 15 kV with a spot size of 4, and with EDS settings as follows: amp time 7.68  $\mu\text{s}$ , dwell time of 50  $\mu\text{s}$ , 512 frames, and a total analysis time of  $\sim 10$  h. Since a larger spot size was chosen to increase signal, the magnification of the mapped area was reduced to lower the

intensity of the beam concentrated on the particle. While the 7.68  $\mu\text{s}$  amp time is recommended for spot analyses rather than EDS mapping, this setting allowed for the measurement of low atomic number elements.

## Gamma-ray spectrometry

Two gamma-ray detectors were used for this study. The first detector is located in the Nuclear and Radiochemistry facility (RC-1) of LANL and is part of the Countroom team's radiometric analysis capability. The Compton Suppression Counter consists of an ORTEC GMX70P4-PLB-S which has a carbon fiber window and a relative efficiency of 65%. The counter is surrounded by 5 NaI(Tl) detectors operating in rejection mode to provide the Compton Suppression. The minimum detectable activity for  $^{137}\text{Cs}$  is 0.01 Bq, and the measurement uncertainty is 5% relative ( $k = 1$ ).

The second detector is located in the Low Activity Investigation Room (LAIR) in a historic Manhattan-project era tunnel in the Los Alamos canyon. The tunnel is more than 100 m long, was built from June 1948 to May 1949, and served various purposes throughout the decades. Today it hosts the Event Verification and Identification Laboratory (EVIL). The LAIR gamma-ray detector is a low-background HPGe detector with a carbon cryostat and a relative efficiency of 60%. EVIL is an underground laboratory with roughly 100 m of water equivalent of overburden. The minimum detectable activity (MDA) for the LAIR detector is 0.08 Bq, the measurement uncertainty is 5% relative.

## Results and discussion

### Particle location and isolation

Autoradiographic imaging of the grass revealed non-uniform distribution of radioactivity in the grass (Fig. 1). Some blades were entirely active, others revealed low activities.

From this image, it becomes apparent that some vegetation specimen contain punctual activities in the buds, e.g. the twig marked as “Twig”. However, the blade of grass on the bottom left (marked with the blue asterisk \*) revealed several hotspots that are not associated with plant specific characteristics. Figure 2 shows a close-up radiographic overlay image (in orange-red false color) with three distinct areas of marginally increased activity.

The spot on the left (sample code J) was chosen for further investigation. In optical microscopy, three black and shiny structures were discovered, two on the front side (Beads #1 and #2, see Fig. 3) of the blade and one on the backside (Bead #3). They are all located next to each other in close vicinity. Bead #3 was the smallest of all three beads

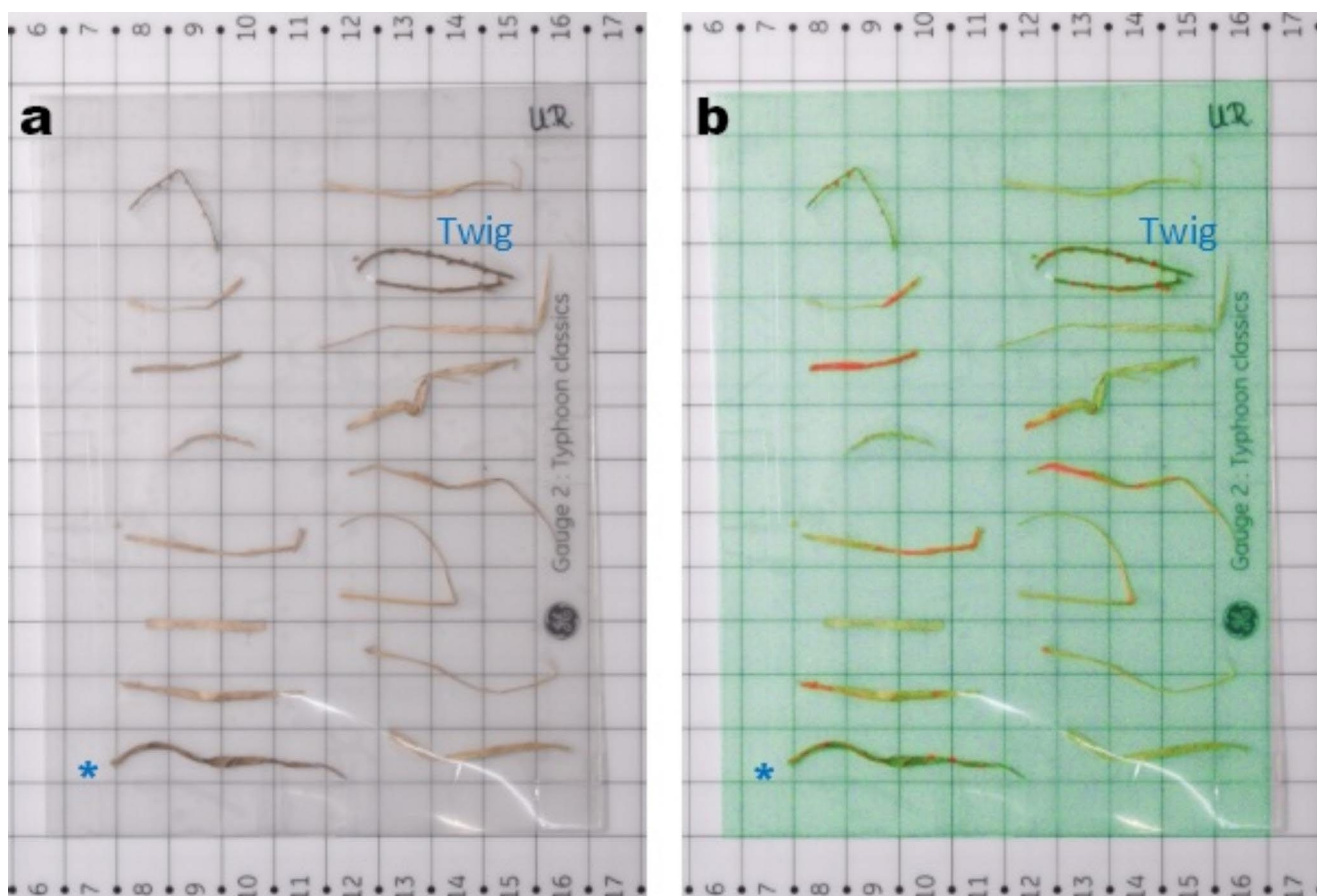


**Fig. 1** Overview of potential vegetation sample candidates (panel “a”) and false-color overlay (red-orange) with the autoradiographic image (panel “b”) of the selected grass blades (exposure time 30 h). The

grid is in inches (1 inch = 2.54 cm). The blade of grass of interest was marked with a blue asterisk \*

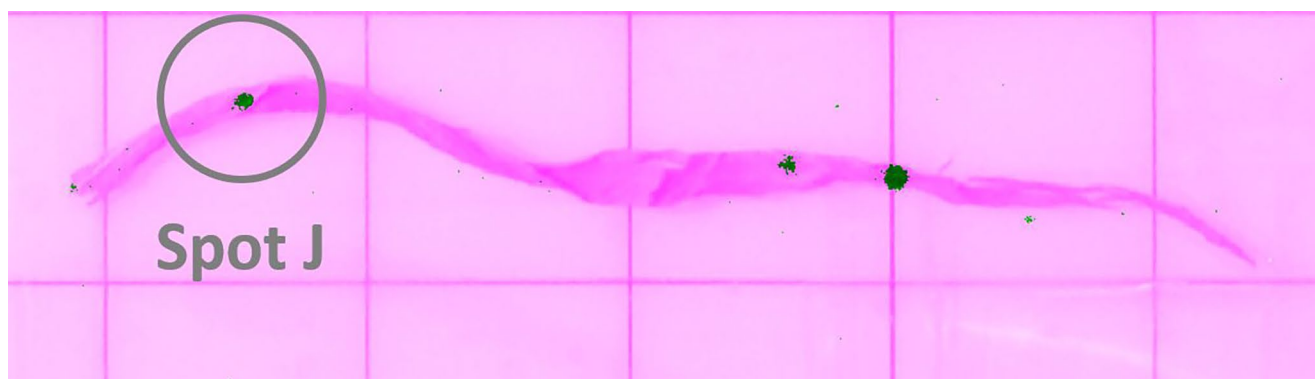


**Fig. 2** Close-up of the radiographic image of the grass blade marked with an asterisk (\*) in Figure 1 in false color overlay (dark green). Spot J was selected for further investigation

and embedded in a dark area of the grass blade. Hence, it did not yield a suitable picture in optical microscopy.

After identification of these three particles of interest, they were extracted with the 1  $\mu\text{m}$  tungsten needle of a micromanipulator and transferred to a silicon wafer. A video of the successful picking of bead #2 is available here: [41]. During extraction, bead #1 popped into at least two smaller

pieces when it was poked with the needle. A video showing this incident is available here: [42] (the breaking of the particle happens at around 1:11 min). Both videos show that the particles are hard and glassy, as the needle slipped off the surface several times. The popping of the particle may have resulted from some tension inside the particle because one larger fragment flew off with some force and could not



**Fig. 3** Beads #1 (top) and #2 (bottom) on hot spot J

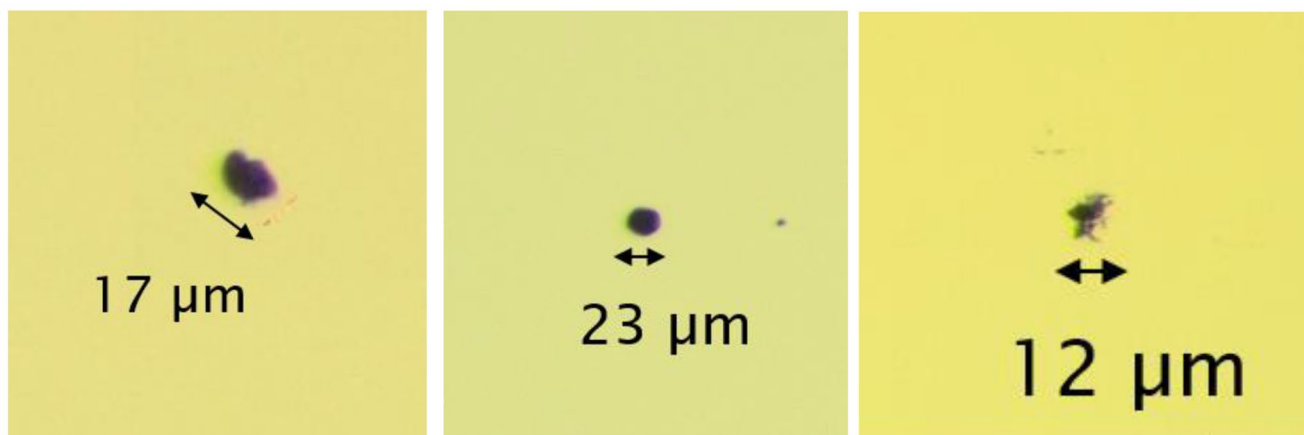


**Fig. 4** Beads #1 (left), #2 (center), and #3 (right) on the silicon wafer after extraction

be found again under the microscope. This lets us assume that the particle may have exhibited high surface tension, which may be explained by a formation of the particle in a hot environment followed by rapid cool-down. It is possible, however, that some sort of crack already pre-existed within the particle when the treatment with tungsten needle triggered its separation.

The largest fragment of bead #1, as well as bead #2 and bead #3 were transferred each to a silicon wafer for subsequent SEM-EDS and gamma-spectrometric investigation. Transfer of particle #3 to the silicon wafer turned out difficult and only succeeded once a small puddle of glue was added to the wafer to allow for the transfer. Figure 4 shows all three particles on their silicon wafers.

### SEM-EDS

Prior to SEM, all wafers were carbon coated using a Cressington 108CarbonA sputter coater. Beads #2 and #3 could be identified in the SEM, however, the fragment of bead #1 could not be found on the silicon wafer. There is a possibility that #1 was lost on the way to SEM. Figure 5 shows bead #2 and #3, respectively.

Both beads #2 and #3 are nearly perfect spheres. Bead #2, as the larger particle, was the primary object of investigation. The surface of #2 is heterogeneous both texturally and in composition with several inclusions adhered to the particle (Figs. 5 and 6). Elemental mapping revealed the matrix of the sample is low in atomic number compared to the silicon substrate. It also indicated the inclusions are higher in atomic number than the particle's matrix. The

**Fig. 5** Beads #2 (left) and #3 (right) under the scanning electron microscope (secondary electron image)

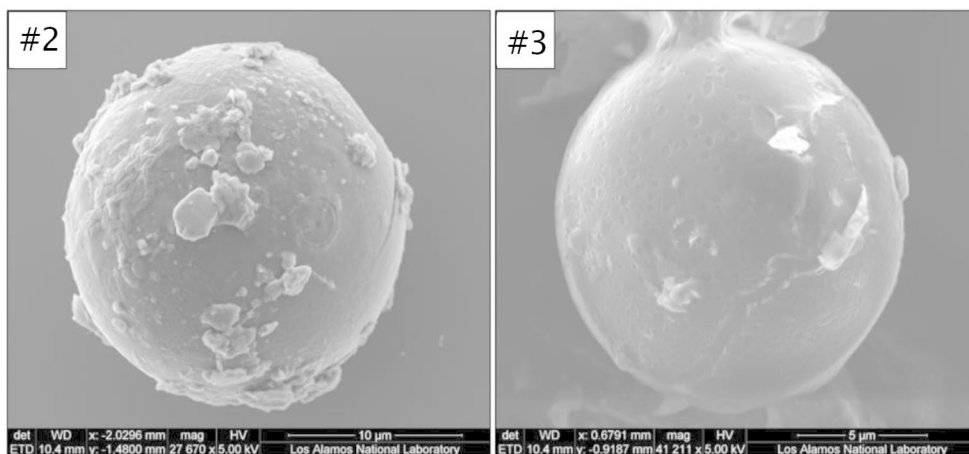
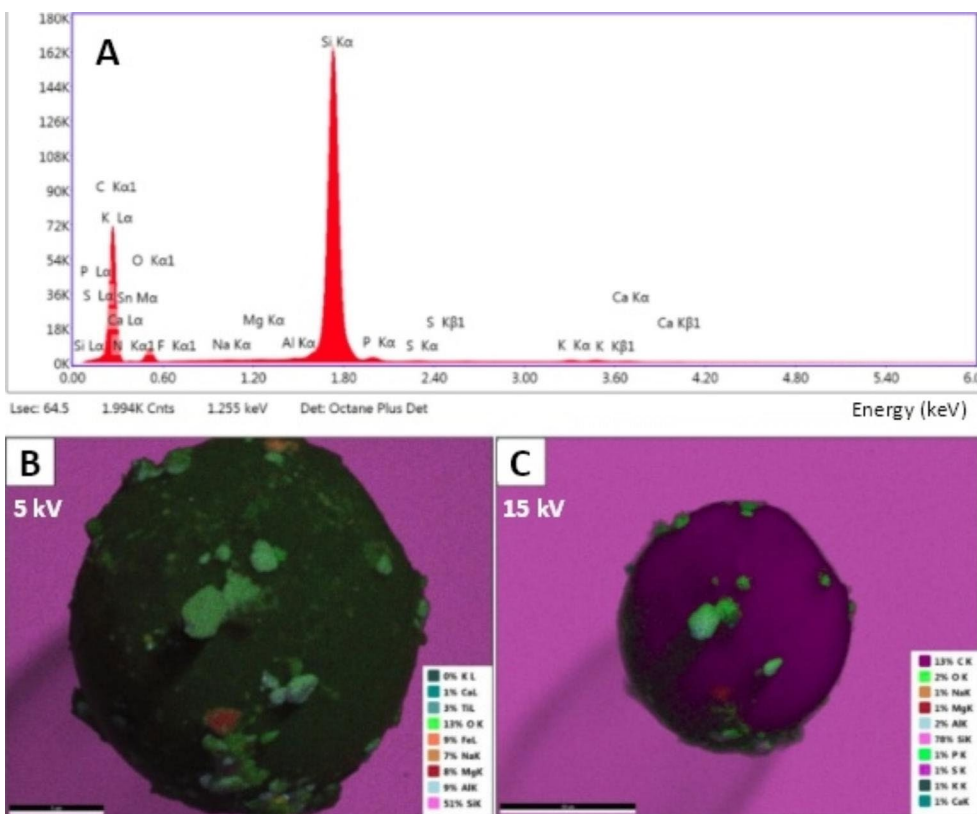


**Fig. 6** EDS spectrum (A) and SEM-EDS map images of bead # 2 at 5 kV (B) and 15 kV (C). Note: maps were taken at different magnifications – map C was taken at a lower magnification to mitigate charging. For major elements: Light pink represents silicon and dark purple represents carbon



5 kV map (Fig. 6B) resolves more of the surface features, while the 15 kV map (Fig. 6C) shows less of the inclusions on the surface and more of the overall composition.

The alleged Sn peak in Fig. 6 (A) is an artefact caused by the “auto ID” of the EDS software. The peak identified as tin (Sn) occurred between the primary peaks for potassium ( $K\alpha = 3.312$  keV) and calcium ( $K\alpha = 3.690$  keV). Further examination of the spectrum revealed the actual peak (located at 3.48 keV) was shifted from the software’s fitted spectrum for tin ( $L\alpha = 3.443$  keV). The actual peak is a sum peak that occurs from two characteristic x-rays of silicon

arriving at the detector at the same time and is hence a common EDS interference.

The most striking result from bead # 2 is the high concentration of carbon. While some of the carbon contribution might be from underestimating the thickness of the carbon coat, the concentration of carbon on the particle is significantly higher than that of the substrate, which should have a similar coating thickness. The presence of carbon is also clearly shown in the 15 kV map of the sample (Fig. 6C). Such high carbon content is rather unusual for Fukushima-derived particles.

**Table 1** Comparison of the main characteristics of the various particle types. Please note that only a selection of references is listed

Particle type	Diameter (μm)	Shape	<sup>137</sup> Cs activity (Bq)*	<sup>134</sup> Cs/ <sup>137</sup> Cs activity ratio*	Reference
A	1–10	spherical	0.1–20	~ 1.04	[18, 27]
B	70–400	non-spherical	30–100	~ 0.93	[27]
C	120	non-spherical	224±3	1.02±0.04	[32]
D	~ 400	non-spherical	3.10·10 <sup>5</sup> (± 92) – 1.27·10 <sup>6</sup> (± 107)	0.954–0.971	[33]
E	12–23	spherical	0.011±0.008	N/A	This study

\* As of March 11, 2011

The surface of bead #3 was found to be completely covered in glue, hence limiting the opportunity for further analytical insight. The glue layer was easily damaged by the beam and contributed significantly to sample contamination, charging, and drift. EDS results indicate the sample is primarily carbon, silicon, and oxygen with some inclusions on the surface, mostly composed of aluminum. Attempts to collect an EDS map failed early into the analysis due to high drift.

### Gamma-ray spectrometry

Prior to particle extraction, spot J exhibited 61±11 mBq <sup>137</sup>Cs in a 3000 min count (as of July 2021). After isolation of the microparticles, bead #2 revealed <sup>137</sup>Cs in activity > uncertainty (1 SD), however just below the critical limit (LC = 10 mBq). The <sup>137</sup>Cs activity of bead #2 was estimated to 9±6 mBq (as of September 2021). Although it cannot be quantified with confidence, the presence of a <sup>137</sup>Cs peak confirms the particle's nuclear origin. The close vicinity of the sampling location to FDNPP makes the Fukushima nuclear accident the obvious source of the particle. However, the particle alone is not responsible for the entire activity in spot J. Bead #3 was measured in various detectors but did not exceed the MDA. Given a particle size of about 23 μm, this yields a specific activity of approx. 1.4 MBq·cm<sup>-3</sup>, which is unusually low compared with CsMP Types A, B, C, and D.

### Comparison with previously described types of particles

When compared with other particle types, the characteristics of Type E particles are unique, as outlined in Table 1. They are unique mainly in size and in low activity. Due to the very low activity levels, <sup>134</sup>Cs activities remained undetectable. Hence, unfortunately, no <sup>134</sup>Cs/<sup>137</sup>Cs ratio could be determined.

## Conclusion

Three microspheres were detected on a blade of grass that was collected in December 2011 in the vicinity of FDNPP. Two of them could be isolated and characterized using SEM-EDS and gamma-ray spectrometry. The particles are nearly spherical and 12–23 μm in diameter. Based on their unique characteristics, in particular when compared with previously described types of Fukushima-derived microparticles, we proclaim a novel Type E microparticle. Type E CsMPs exhibit the following characteristics:

- Type E microparticles found in this study are 12–23 μm in diameter and hence about 5–10 times larger than Type A, about 5–10 times smaller than Types B and C, and they are at least 25 times smaller than Type D.
- Type E microparticles are nearly spherical like Type A, but unlike Type B, C, and D particles.
- Type E microparticles are compositionally distinct from Type A, B, and C with very low Cs content and very high C content. There are inclusions (compositionally distinct with higher atomic number) that are embedded in their surface. The high carbon content resembles the composition of type D particles.
- Type E microparticles exhibit extremely low, barely detectable <sup>137</sup>Cs activities. They are at least 10 times lower in <sup>137</sup>Cs activity than Type A and about 10,000 times lower than Types B and C and at least 10<sup>8</sup> times lower than the large particles of Type D.
- Specific activities in Type E microparticles are in the MBq·cm<sup>-3</sup> range, hence at least 10 times lower than every other type of FDNPP particle that has been described so far.
- Type E microparticles exhibit high surface tension, as one specimen almost explosively broke into pieces when handled with a tungsten needle. In combination with the spherical shape, this may indicate that their origin may have been a hot environment (possibly in combination with rapid cool-down).

**Acknowledgements** We gratefully acknowledge funding of this study by *Deutsche Forschungsgemeinschaft* (DFG) (project no. 419819104) and partial support by JSPS KAKENHI 19K12306. This work was supported by the US Department of Energy through the Los Alamos National Laboratory. Los Alamos National Laboratory is operated by Triad National Security, LLC, for the National Nuclear Security Administration of U.S. Department of Energy (Contract No. 89233218CNA000001). This publication is LA-UR-22-24258.

**Funding** Open Access funding enabled and organized by Projekt DEAL.

**Open Access** This article is licensed under a Creative Commons Attribution 4.0 International License, which permits use, sharing, adaptation, distribution and reproduction in any medium or format,

as long as you give appropriate credit to the original author(s) and the source, provide a link to the Creative Commons licence, and indicate if changes were made. The images or other third party material in this article are included in the article's Creative Commons licence, unless indicated otherwise in a credit line to the material. If material is not included in the article's Creative Commons licence and your intended use is not permitted by statutory regulation or exceeds the permitted use, you will need to obtain permission directly from the copyright holder. To view a copy of this licence, visit <http://creativecommons.org/licenses/by/4.0/>.

## References

- Steinhauser G, Brandl A, Johnson TE (2014) Comparison of the Chernobyl and Fukushima nuclear accidents: A review of the environmental impacts. *Sci Total Environ* 470–471:800–817. doi:<https://doi.org/10.1016/j.scitotenv.2013.10.029>
- Russell BC, Croudace IW, Warwick PE, Milton JA (2014) Determination of precise  $^{135}\text{Cs}/^{137}\text{Cs}$  ratio in environmental samples using sector field inductively coupled plasma mass spectrometry. *Anal Chem* 86:8719–8726. doi:<https://doi.org/10.1021/ac501894a>
- Zheng J, Tagami K, Bu W, Uchida S, Watanabe Y, Kubota Y, Fuma S, Ihara S (2014) Isotopic ratio of  $^{135}\text{Cs}/^{137}\text{Cs}$  as a new tracer of radiocesium released from the Fukushima nuclear accident. *Environ Sci Technol* 48(10):5433–5438
- Russell BC, Croudace IW, Warwick PE (2015) Determination of  $^{135}\text{Cs}$  and  $^{137}\text{Cs}$  in environmental samples: A review. *Anal Chim Acta* 890:7–20. doi:<https://doi.org/10.1016/j.aca.2015.06.037>
- Zok D, Blenke T, Reinhard S, Sprott S, Kegler F, Syrbe L, Querfeld R, Takagai Y, Drozdov V, Chyzhevskiy I, Kirieiev S, Schmidt B, Adlassnig W, Wallner G, Dubchak S, Steinhauser G (2021) Determination of characteristic vs anomalous  $^{135}\text{Cs}/^{137}\text{Cs}$  isotopic ratios in radioactively contaminated environmental samples. *Environ Sci Technol* 55(8):1984–4991. doi:<https://doi.org/10.1021/acs.est.1c00180>
- Hamada N, Ogino H (2012) Food safety regulations: what we learned from the Fukushima nuclear accident. *J Environ Radioact* 111:83–99. doi:<https://doi.org/10.1016/j.jenvrad.2011.08.008>
- Chino M, Nakayama H, Nagai H, Terada H, Katata G, Yamazawa H (2011) Preliminary estimation of release amounts of  $^{131}\text{I}$  and  $^{137}\text{Cs}$  accidentally discharged from the Fukushima Daiichi nuclear power plant into the atmosphere. *J Nucl Sci Technol* 48:1129–1134. doi:<https://doi.org/10.3327/jnst.48.1129>
- Ten Hoeve JE, Jacobson MZ (2012) Worldwide health effects of the Fukushima Daiichi nuclear accident. *Energy Environ Sci* 5(9):8743–8757. doi:<https://doi.org/10.1039/c2ee22019a>
- Stohl A, Seibert P, Wotawa G, Arnold D, Burkhardt JF, Eckhardt S, Tapia C, Vargas A, Yasunari TJ (2012) Xenon-133 and caesium-137 releases into the atmosphere from the Fukushima Dai-ichi nuclear power plant: determination of the source term, atmospheric dispersion, and deposition. *Atmos Chem Phys* 12(5):2313–2343. doi:<https://doi.org/10.5194/acp-12-2313-2012>
- Merz S, Steinhauser G, Hamada N (2013) Anthropogenic radionuclides in Japanese food: environmental and legal implications. *Environ Sci Technol* 47(3):1248–1256. doi:<https://doi.org/10.1021/es3037498>
- Steinhauser G (2018) Anthropogenic radioactive particles in the environment. *J Radioanal Nucl Chem* 318(3):1629–1639. doi:<https://doi.org/10.1007/s10967-018-6268-4>
- Kashparov V, Salbu B, Levchuk S, Protsak V, Maloshtan I, Simonucci C, Courbet C, Nguyen HL, Sanzharova N, Zabrotsky V (2019) Environmental behaviour of radioactive particles from Chernobyl. *J Environ Radioact* 208–209:106025. doi:<https://doi.org/10.1016/j.jenvrad.2019.106025>
- Salbu B, Kashparov V, Lind OC, Garcia-Tenorio R, Johansen MP, Child DP, Roos P, Sancho C (2018) Challenges associated with the behaviour of radioactive particles in the environment. *J Environ Radioact* 186:101–115. doi:<https://doi.org/10.1016/j.jenvrad.2017.09.001>
- Yoschenko V, Ohkubo T, Kashparov V (2018) Radioactive contaminated forests in Fukushima and Chernobyl. *J For Res* 23(1):3–14. doi:<https://doi.org/10.1080/13416979.2017.1356681>
- Nakajima H, Fujiwara M, Tanihata I (2012) What can be seen in autoradiography image of leaves? *Mod Chem*:34–37 (in Japanese)
- Sakamoto F, Ohnuki T, Kozai N, Igarashi S, Yamazaki S, Yoshida Z, Tanaka S (2012) Local area distribution of fallout radionuclides from the Fukushima Daiichi Nuclear Power Plant determined by autoradiography analysis. *J Atom Energy Soc Jpn* 11:1–7 (in Japanese)
- Adachi K, Kajino M, Zaizen Y, Igarashi Y (2013) Emission of spherical cesium-bearing particles from an early stage of the Fukushima nuclear accident. *Sci Rep* 3:2554. doi:<https://doi.org/10.1038/srep02554>
- Tang P, Kita K, Igarashi Y, Satou Y, Hatanaka K, Adachi K, Kinase T, Ninomiya K, Shinohara A (2022) Atmospheric resuspension of insoluble radioactive cesium-bearing particles found in the difficult-to-return area in Fukushima. *Progress in Earth and Planetary Science* 9(1):17. doi:<https://doi.org/10.1186/s40645-022-00475-6>
- Abe Y, Iizawa Y, Terada Y, Adachi K, Igarashi Y, Nakai I (2014) Detection of uranium and chemical state analysis of individual radioactive microparticles emitted from the Fukushima nuclear accident using multiple synchrotron radiation x-ray analyses. *Anal Chem* 86(17):8521–8525. doi:<https://doi.org/10.1021/ac501998d>
- Ochiai A, Imoto J, Suetake M, Komiya T, Furuki G, Ikehara R, Yamasaki S, Law GTW, Ohnuki T, Grambow B, Ewing RC, Utsunomiya S (2018) Uranium Dioxides and Debris Fragments Released to the Environment with Cesium-Rich Microparticles from the Fukushima Daiichi Nuclear Power Plant. *Environ Sci Technol* 52(5):2586–2594. doi:<https://doi.org/10.1021/acs.est.7b06309>
- Imoto J, Ochiai A, Furuki G, Suetake M, Ikehara R, Horie K, Takehara M, Yamasaki S, Nanba K, Ohnuki T, Law GTW, Grambow B, Ewing RC, Utsunomiya S (2017) Isotopic signature and nano-texture of cesium-rich micro-particles: Release of uranium and fission products from the Fukushima Daiichi Nuclear Power Plant. *Sci Rep* 7(1):5409. doi:<https://doi.org/10.1038/s41598-017-05910-z>
- Reinoso-Maset E, Brown J, Pettersen MN, Steenhuisen F, Tetteh A, Wada T, Hinton TG, Salbu B, Lind OC (2020) Linking heterogeneous distribution of radiocaesium in soils and pond sediments in the Fukushima Daiichi exclusion zone to mobility and potential bioavailability. *J Environ Radioact* 211:106080. doi:<https://doi.org/10.1016/j.jenvrad.2019.106080>
- Martin PG, Satou Y, Griffiths I, Richards D, Scott T (2017) Analysis of External Surface Irregularities on Fukushima-Derived Fallout Particles. *Front Energy Res* 5. doi:<https://doi.org/10.3389/fenrg.2017.00025>
- Hidaka A (2019) Formation mechanisms of insoluble Cs particles observed in Kanto district four days after Fukushima Daiichi NPP accident. *J Nucl Sci Technol* 56(9–10):831–841. doi:<https://doi.org/10.1080/00223131.2019.1583611>
- Ishizuka M, Mikami M, Tanaka TY, Igarashi Y, Kita K, Yamada Y, Yoshida N, Toyoda S, Satou Y, Kinase T, Ninomiya K, Shinohara A (2017) Use of a size-resolved 1-D resuspension scheme to evaluate resuspended radioactive material associated with



- mineral dust particles from the ground surface. *J Environ Radioact* 166:436–448. doi:<https://doi.org/10.1016/j.jenvrad.2015.12.023>
26. Hagiwara H, Kondo K (2022) The formation mechanism of radiocesium-bearing microparticles derived from the Fukushima Dai-ichi nuclear power plant using electron microscopy. *J Radioanal Nucl Chem*. doi:<https://doi.org/10.1007/s10967-022-08434-7>
  27. Satou Y, Sueki K, Sasa K, Yoshikawa H, Nakama S, Minowa H, Abe Y, Nakai I, Ono T, Adachi K, Igarashi Y (2018) Analysis of two forms of radioactive particles emitted during the early stages of the Fukushima Dai-ichi Nuclear Power Station accident. *Geochem J* 52(2):137–143. doi:<https://doi.org/10.2343/geochemj.2.0514>
  28. Hagiwara H, Funaki H, Shiribiki N, Kanno M, Sanada Y (2022) Characterization of radiocesium-bearing microparticles with different morphologies in soil around the Fukushima Daiichi nuclear power plant. *J Radioanal Nucl Chem* 331:415–426. doi:<https://doi.org/10.1007/s10967-021-08061-8>
  29. Ikehara R, Morooka K, Suetake M, Komiya T, Kurihara E, Takehara M, Takami R, Kino C, Horie K, Takehara M, Yamasaki S, Ohnuki T, Law GTW, Bower W, Grambow B, Ewing RC, Utsunomiya S (2020) Abundance and distribution of radioactive cesium-rich microparticles released from the Fukushima Daiichi Nuclear Power Plant into the environment. *Chemosphere* 241:125019. doi:<https://doi.org/10.1016/j.chemosphere.2019.125019>
  30. Igarashi Y, Kogure T, Kurihara Y, Miura H, Okumura T, Satou Y, Takahashi Y, Yamaguchi N (2019) A review of Cs-bearing microparticles in the environment emitted by the Fukushima Dai-ichi Nuclear Power Plant accident. *J Environ Radioact* 205–206:101–118. doi:<https://doi.org/10.1016/j.jenvrad.2019.04.011>
  31. Chino M, Terada H, Nagai H, Katata G, Mikami S, Torii T, Saito K, Nishizawa Y (2016) Utilization of  $^{134}\text{Cs}/^{137}\text{Cs}$  in the environment to identify the reactor units that caused atmospheric releases during the Fukushima Daiichi accident. *Sci Rep* 6(1):31376. doi:<https://doi.org/10.1038/srep31376>
  32. Zhang Z, Igarashi J, Satou Y, Ninomiya K, Sueki K, Shinohara A (2019) Activity of  $^{90}\text{Sr}$  in fallout particles collected in the difficult-to-return zone around the Fukushima Daiichi nuclear power plant. *Environ Sci Technol* 53(10):5868–5876. doi:<https://doi.org/10.1021/acs.est.8b06769>
  33. Morooka K, Kurihara E, Takehara M, Takami R, Fueda K, Horie K, Takehara M, Yamasaki S, Ohnuki T, Grambow B, Law GTW, Ang JWL, Bower WR, Parker J, Ewing RC, Utsunomiya S (2021) New highly radioactive particles derived from Fukushima Daiichi Reactor Unit 1: Properties and environmental impacts. *Sci Total Environ* 773:145639. doi:<https://doi.org/10.1016/j.scitotenv.2021.145639>
  34. Kurihara E, Takehara M, Suetake M, Ikehara R, Komiya T, Morooka K, Takami R, Yamasaki S, Ohnuki T, Horie K, Takehara M, Law GTW, Bower W, Mosselmans W, Warnicke JF, Grambow B, Ewing B, Utsunomiya RC S (2020) Particulate plutonium released from the Fukushima Daiichi meltdowns. *Sci Total Environ* 743:140539. doi:<https://doi.org/10.1016/j.scitotenv.2020.140539>
  35. Jaegler H, Pointurier F, Onda Y, Angulo JF, Griffiths NM, Moureau A, Faure A-L, Marie O, Hubert A, Evrard O (2019) Method for detecting and characterising actinide-bearing microparticles in soils and sediment of the Fukushima Prefecture, Japan. *J Radioanal Nucl Chem* 321(1):57–69. doi:<https://doi.org/10.1007/s10967-019-06575-w>
  36. Diacre A, Fichet P, Sardini P, Donnard J, Fauré A-L, Marie O, Shozugawa K, Susset M, Hori M, Tsutomu T, Pointurier F, Evrard O (2022) Comparison of techniques to localise U-bearing particles in environmental samples. *J Radioanal Nucl Chem*. doi:<https://doi.org/10.1007/s10967-022-08229-w>
  37. Ikehara R, Suetake M, Komiya T, Furuki G, Ochiai A, Yamasaki S, Bower WR, Law GTW, Ohnuki T, Grambow B, Ewing RC, Utsunomiya S (2018) Novel method of quantifying radioactive cesium-rich microparticles (CsMPs) in the environment from the Fukushima Daiichi nuclear power plant. *Environ Sci Technol* 52(11):6390–6398. doi:<https://doi.org/10.1021/acs.est.7b06693>
  38. Bosco H, Hamann L, Kneip N, Raiwa M, Weiss M, Wendt K, Walther C New horizons in microparticle forensics: Actinide imaging and detection of  $^{238}\text{Pu}$  and  $^{242}\text{mAm}$  in hot particles. *Science Advances* 7 (44):eabj1175. doi:<https://doi.org/10.1126/sciadv.abj1175>
  39. Steinhauser G, Schauer V, Shozugawa K (2013) Concentration of strontium-90 at selected hot spots in Japan. *PLoS ONE* 8(3):e57760. doi:<https://doi.org/10.1371/journal.pone.0057760>
  40. Schneider S, Walther C, Bister S, Schauer V, Christl M, Sinal H-A, Shozugawa K, Steinhauser G (2013) Plutonium release from Fukushima Daiichi fosters the need for more detailed investigations. *Sci Rep* 3:2988. doi:<https://doi.org/10.1038/srep02988>
  41. Supplementary Material (2022) Picking a radioactive Fukushima-particle under the microscope. LA-UR-21-29686, Approved for public release; distribution is unlimited. <https://youtu.be/W3sIM30KLR4>
  42. Supplementary Material (2022) Popping of a Fukushima-derived particle during picking with a tungsten needle. LA-UR-22-22988. Approved for public release; distribution is unlimited. <https://youtu.be/jtpSYfTNJEI>

**Publisher's Note** Springer Nature remains neutral with regard to jurisdictional claims in published maps and institutional affiliations.